Stanford Exploration Project, Report 102, October 25, 1999, pages 1–??

Offset plane waves vs. common-azimuth migration for sub-salt imaging

Biondo Biondi[1]

keywords: *depth migration, wave-propagation, wave equation*

ABSTRACT

Offset plane wave migration and common-azimuth migration are among the most promising wave-equation migration methods for efficiently imaging 3-D marine data sets. Offset plane wave migration has some computational advantages over common-azimuth migration, but common-azimuth is more accurate. Sub-salt images produced by common-azimuth migration are better focused than the corresponding images produced by offset plane wave migration. These differences can be attributed to an approximation intrinsic to offset plane wave migration: the offset plane wave components are downward continued separately, instead of being allowed to mix as they should be in media with laterally varying velocity.

Offset plane wave migration also approximates the cross-line offset ray parameter of the plane-waves with zero. A theoretical analysis of the migration errors caused by this approximation is confirmed by the imaging results. The shallow reflectors dipping at 45 degrees with respect to the acquisition axes are poorly imaged by offset plane wave migration.

INTRODUCTION

In a previous report (Biondi, 1999a) I showed that common-azimuth prestack migration produces better sub-salt images than a single arrival Kirchhoff migration. In this report Vaillant and Sava (1999) show excellent preliminary results of common-azimuth migration of a salt body in the North Sea, and again favorable comparison with the results obtained using a most-energetic arrival Kirchhoff-like migration. The evidence is mounting that wave-equation migration, even when applied using approximate methods as common-azimuth, has the potential to produce better images than Kirchhoff methods when strong lateral velocity variations cause multi-pathing of the reflected energy. Full-volume imaging of deep targets when steep reflectors require huge migration aperture is another area of applications for efficient wave-equation migration methods that is gaining interest. In these cases the cost of Kirchhoff migration is large, and downward continuation methods become attractive from the computational point of

[1]**email:** biondo@sep.stanford.edu

view.

Offset plane wave migration (Ottolini and Claerbout, 1984; Mosher et al., 1997) is another approximate wave-equation method that has been recently applied to the migration of 3-D prestack marine data. Offset plane wave migration is related to common-azimuth migration, and has similar computational complexity. Therefore, a comparison between the two is of both practical and theoretical interest. Both methods have been applied to marine data transformed to common-azimuth data, and achieve computational efficiency by restricting the computational domain to a 4-D space from the 5-D space that is required by full downward continuation. Offset plane wave migration has the additional computational advantage that it can be performed as several independent migrations of 3-D cubes, while common-azimuth migration requires, at least in principle, to be performed on the whole 4-D data set simultaneously. This difference means that offset-plane wave migration requires less computations (about 10%) and has lower minimum-memory requirements to run efficiently. Though, for both methods the memory requirements are manageable on modern computers because the computational domain is further decomposed in temporal-frequency components. On the other hand, downward continuing the offset plane waves separately introduces errors when migration velocity has strong lateral variations, as in the case of sub-salt imaging. In this paper I show example of migration errors related to this approximation.

Another approximation introduced by offset plane wave migration is neglecting the cross-line component of the offset plane wave ray parameter vector and setting its value equal to zero. In this paper, I study the effects of this approximation with a theoretical analysis and with migration results. The approximation affects mostly the migration accuracy of reflections recorded at large offset from shallow reflectors with dips oriented at an angle with respect to the acquisition axes. The demonstration of this phenomenon is quite simple. It is based on the analytical proof that in constant velocity neglecting the cross-line component of the offset plane wave ray parameter vector is equivalent to reversing the correct order of two-pass migration. The correct order for two-pass prestack migration is: in-line prestack migration followed by cross-line zero-offset migration (Biondi, 1999b; Rosa et al., 1999). On the contrary, offset plane wave migration is equivalent to performing a cross-line zero offset migration followed by an in-line prestack migration.

The reversing of the correct order of two-pass migration produces the largest errors for shallow reflectors and large offsets. The errors become negligible for deep reflectors. Offset plane wave migration is thus a valuable tool for producing full-volume images of deep targets below relatively mild velocity functions, such as the imaging of salt flanks in deep waters. On the contrary, when shallow reflectors are important, or when strong lateral velocity variations are present, common-azimuth migration produces better images.

EFFICIENT WAVE-EQUATION MIGRATIONS OF COMMON-AZIMUTH DATA

The full downward continuation of 3-D prestack data can be expressed in the frequency-wavenumber domain by the following phase-shift operator

$$D_{z+\Delta z}(\omega, \mathbf{k_m}, \mathbf{k_h}) \approx D_z(\omega, \mathbf{k_m}, \mathbf{k_h})\, e^{-ik_z \Delta z}, \tag{1}$$

where ω is the temporal frequency, $\mathbf{k_m}$ is the midpoint-wavenumber vector, $\mathbf{k_h}$ is the offset-wavenumber vector, and $v(\mathbf{s},z)$ and $v(\mathbf{g},z)$ are respectively the velocity at the source and receivers locations. The vertical wavenumber k_z is given by the Double Square Root (DSR),

$$\begin{aligned} k_z &= \sqrt{\frac{\omega^2}{v^2(\mathbf{s},z)} - \frac{1}{4}\left[\left(k_{x_m} - k_{x_h}\right)^2 + \left(k_{y_m} - k_{y_h}\right)^2\right]} \\ &+ \sqrt{\frac{\omega^2}{v^2(\mathbf{g},z)} - \frac{1}{4}\left[\left(k_{x_m} + k_{x_h}\right)^2 + \left(k_{y_m} + k_{y_h}\right)^2\right]}. \end{aligned} \tag{2}$$

This operator is a function of the cross-line component of the offset wavenumber k_{y_h}, while common-azimuth data are independent of k_{y_h} because they are different from zero only at $y_h = 0$. Therefore, the exact full downward continuation is performed by applying a 5-D operator on a data set that is only 4-D. While accurate, this procedure is tremendously wasteful of computational efforts, because only a small subset of the 5-D wavefield contributes to the final image. The final image is formed by extracting the zero-offset cube from the downward-continued wavefield. This data extraction is equivalent to the summation of the wavefield along both offset-wavenumber axes. Most of the wavefield components destructively interfere in the imaging step. In fact, only a 4-D slice of the 5-D wavefield contributes to the image when no multipathing occurs, such as in constant velocity or in a vertically layered media. Even when multipathing occurs, most of the wavefield components destructively interfere in the imaging step.

It is therefore natural to limit the computational cost by reducing the dimensionality of the downward continuation operator from 5-D to 4-D. Both common-azimuth migration and offset plane wave migration achieve this goal, though in different ways.

Common-azimuth downward continuation

Common azimuth migration reduces the dimensionality of the continuation operator by restricting the wavefield to be common-azimuth at every depth level. It can be demonstrated that this approximation is exact in constant velocity (Biondi and Palacharla, 1996). This geometric condition is equivalent to selecting one particular value for the cross-line component of the offset wavenumber k_{y_h} as a function of the frequency ω, the other wavenumbers $(k_{x_m}, k_{y_m}, k_{x_h})$, and the propagation velocities $[v(\mathbf{g},z), v(\mathbf{s},z))]$. This value for k_{y_h} is then substituted into the expression for the full DSR of equation (2), to obtain the common-azimuth downward-continuation operator.

The analytical expression for k_{y_h} can be either obtained by geometric considerations or by a stationary-phase analysis, and is given as

$$\widehat{k_{y_h}} = k_{y_m} \frac{\sqrt{\frac{\omega^2}{v^2(\mathbf{g},z)} - \frac{1}{4}\left(k_{x_m}+k_{x_h}\right)^2} - \sqrt{\frac{\omega^2}{v^2(\mathbf{s},z)} - \frac{1}{4}\left(k_{x_m}-k_{x_h}\right)^2}}{\sqrt{\frac{\omega^2}{v^2(\mathbf{g},z)} - \frac{1}{4}\left(k_{x_m}+k_{x_h}\right)^2} + \sqrt{\frac{\omega^2}{v^2(\mathbf{s},z)} - \frac{1}{4}\left(k_{x_m}-k_{x_h}\right)^2}}. \tag{3}$$

The common-azimuth dispersion relation that is obtained by substituting equation (3) into equation (2) can be recast, after some algebraic manipulations, as a cascade of two dispersion relations. The first performs 2-D prestack downward-continuation along the in-line direction:

$$k_{z_x} = \sqrt{\frac{\omega^2}{v^2(\mathbf{s},z)} - \frac{1}{4}\left(k_{x_m}-k_{x_h}\right)^2} + \sqrt{\frac{\omega^2}{v^2(\mathbf{g},z)} - \frac{1}{4}\left(k_{x_m}+k_{x_h}\right)^2}, \tag{4}$$

and the second performs 2-D zero-offset downward continuation along the cross-line axis:

$$\widehat{k_z} = \sqrt{k_{z_x}^2 - k_{y_m}^2}. \tag{5}$$

This rewriting of the common-azimuth dispersion connects common-azimuth migration to the theory of two-pass migration. In the special case of constant velocity, this connection is easily established through Stolt migration formalism (Stolt, 1978). Stolt migration is performed by stretching the temporal frequency (or the vertical wavenumber axis) according to the dispersion relation used for downward continuation. The cascade of two Stolt migrations is equivalent to a single Stolt migration that uses the cascade of the two dispersion relations.

In particular, common-azimuth Stolt migration is equivalent to in-line prestack Stolt migration followed by Stolt cross-line zero-offset migration. In the next section, we will show that this two-pass migration is also kinematically equivalent to the exact full-prestack migration of common-azimuth data.

Offset plane-wave downward continuation

Offset plane wave migration reduces the computational complexity of downward continuation of common-azimuth data one step further than common-azimuth migration does. It approximates the application of the full 5-D operator expressed in equation (2) with the application of several 3-D downward continuation operators. These 3-D operators are applied to common-azimuth data after plane-wave decomposition along the offset axis. The first step of the method is thus the decomposition of the common-azimuth data into offset plane waves. Each plane wave is then independently downward continued. Full downward continuation of offset plane waves could be performed by applying following operator

$$D_{z+\Delta z}(\omega, \mathbf{k_m}, \mathbf{p_h}) \approx D_z(\omega, \mathbf{k_m}, \mathbf{p_h})\, e^{-ik_z \Delta z}, \tag{6}$$

where the vertical wavenumber k_z is now function of the offset plane wave parameters $p_{x_h} = k_{x_h}/\omega$ and $p_{y_h} = k_{y_h}/\omega$; that is,

$$\begin{aligned} k_z &= \sqrt{\frac{\omega^2}{v^2(\mathbf{s},z)} - \frac{1}{4}\left[\left(k_{x_m} - \omega p_{x_h}\right)^2 + \left(k_{y_m} - \omega p_{y_h}\right)^2\right]} \\ &+ \sqrt{\frac{\omega^2}{v^2(\mathbf{g},z)} - \frac{1}{4}\left[\left(k_{x_m} + \omega p_{x_h}\right)^2 + \left(k_{y_m} + \omega p_{y_h}\right)^2\right]}. \end{aligned} \tag{7}$$

Strictly speaking, only in vertically layered media can each plane wave be downward continued independently. The plane waves should be allowed to mix at each depth step when lateral velocity variations occur. Therefore, the computationally attractive feature of imaging each plane wave independently also causes limitations in accuracy. These limitations are difficult to study analytically, and thus in a following section I will analyze their effects by comparing migration results below a complex overburden (eg. a salt body).

In practice, because common-azimuth data has no cross-line offset axis, the plane wave decomposition is performed only as a function of the in-line offset ray parameter p_{x_h}, and the cross-line offset ray parameter p_{y_h} is assumed to be zero. This assumption introduces another approximation in the migration operator, that can be studied analytically.

When p_{y_h} is set to zero, equation (7) becomes:

$$\begin{aligned} \overline{k_z} &= \sqrt{\frac{\omega^2}{v^2(\mathbf{s},z)} - \frac{k_{y_m}^2}{4} - \frac{1}{4}\left(k_{x_m} - \omega p_{x_h}\right)^2} \\ &+ \sqrt{\frac{\omega^2}{v^2(\mathbf{g},z)} - \frac{k_{y_m}^2}{4} - \frac{1}{4}\left(k_{x_m} + \omega p_{x_h}\right)^2}. \end{aligned} \tag{8}$$

This equation is equivalent to the offset plane wave equation presented by Mosher et al. (1997). [2]

It is easy to verify that if we assume $v(\mathbf{s},z) \approx v(\mathbf{g},z) = v(\mathbf{m},z)$, the dispersion relation of equation (8) can be expressed as the cascade of a zero-offset downward continuation along the cross-line direction:

$$k_{z_y} = \sqrt{\frac{\omega^2}{v^2(\mathbf{m},z)} - \frac{k_{y_m}^2}{4}}, \tag{9}$$

and prestack downward continuation along the in-line direction:

$$\overline{k_z} = \sqrt{k_{z_y}^2 - \frac{1}{4}\left(k_{x_m} - \omega p_{x_h}\right)^2} + \sqrt{k_{z_y}^2 - \frac{1}{4}\left(k_{x_m} + \omega p_{x_h}\right)^2}. \tag{10}$$

The interpretation of this decomposition is similar to the one discussed above for common-azimuth migration. A constant velocity offset plane wave migration that uses the dispersion relation of equation (8) is equivalent to a constant-velocity cross-line zero-offset migration, followed by a constant-velocity in-line prestack migration. The order between these migrations is thus reversed with respect to the correct order. We analyze the implications of this order reversal in the following section.

[2] Equation (8) is the same as equation (13) in their abstract.

COMPARING CONSTANT-VELOCITY MIGRATION OPERATORS

In constant velocity the summation surface of 3-D prestack migration is

$$\begin{aligned} t_D &= \sqrt{\frac{z_\xi^2}{V^2} + \frac{\left(x_\xi - x_m + x_h\right)^2 + \left(y_\xi - y_m\right)^2}{V^2}} \\ &+ \sqrt{\frac{z_\xi^2}{V^2} + \frac{\left(x_\xi - x_m - x_h\right)^2 + \left(y_\xi - y_m\right)^2}{V^2}}, \end{aligned} \tag{11}$$

where (z_ξ, x_ξ, y_ξ) are the coordinates of the image point, (x_m, y_m) are the midpoint coordinates in data space, x_h is the in-line offset in data space, t_D is recording time in data space, and V is the medium velocity.

It is easy to verify that this summation surface is equivalent to the summation surface defined by the cascade of the two following expressions:

$$t_D = \sqrt{\frac{z_{\bar{x}}^2}{V^2} + \frac{\left(x_\xi - x_m + x_h\right)^2}{V^2}} + \sqrt{\frac{z_{\bar{x}}^2}{V^2} + \frac{\left(x_\xi - x_m - x_h\right)^2}{V^2}}, \tag{12}$$

$$z_{\bar{x}} = \sqrt{z_\xi^2 + \left(y_\xi - y_m\right)^2}. \tag{13}$$

Equation (12) defines the summation path for 2-D prestack migration and corresponds to the dispersion relation in equation (4). Equation (13) defines the summation path for 2-D zero-offset migration and corresponds to the dispersion relation in equation (5). The straightforward interpretation of this result is that two-pass migration, in the correct order, is equivalent to full prestack migration, when the velocity is constant.

The dispersion relations of offset plane wave migration [equation (9) and equation (10)] respectively correspond to the following summation paths

$$t_D = \sqrt{\frac{z_{\bar{y}}^2}{V^2} + \frac{4\left(y_\xi - y_m\right)^2}{V^2}}, \tag{14}$$

$$z_{\bar{y}} = \sqrt{z_\xi^2 + \left(x_\xi - x_m + x_h\right)^2} + \sqrt{z_\xi^2 + \left(x_\xi - x_m - x_h\right)^2}. \tag{15}$$

The summation surface of offset plane wave migration is thus equivalent the cascade of these two paths. As noted before, the order of the two migration is reversed with respect to the correct one, and thus errors are introduced in the migration operator.

Figure 1 provides an intuitive understanding of the approximations involved in reversing the order of the migrations. The grey surface shown in the left panel of Figure 1 is the summation surface that should be used to image a diffractor at 500 m depth from data at a constant offset of 4,000 m, and assuming a constant velocity of 2,500 m/s. Two sets of contour lines are superimposed onto the surface. The inner set of contour lines corresponds to the exact summation surface, while the outer one corresponds to the surface defined by cascading the paths defined in equation (14) and equation (15). The right panel of Figure 1 shows the

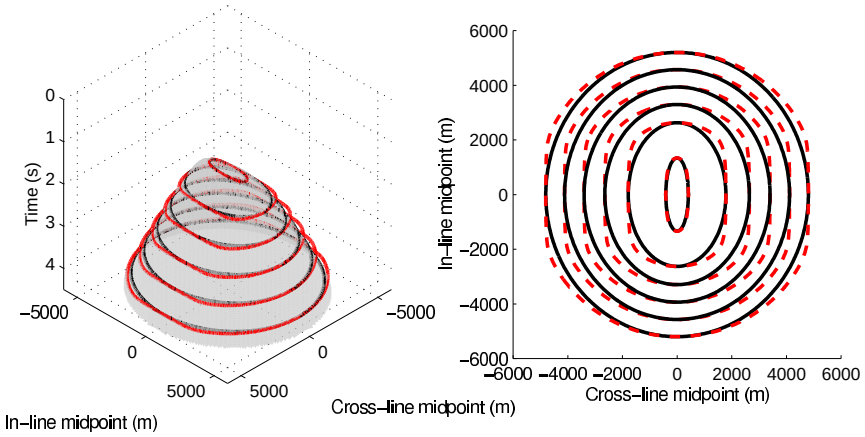

Figure 1: The grey surface shown in the left panel is the exact summation surface to image a diffractor at 500 m depth from data at a constant offset of 4,000 m, and assuming a constant velocity of 2,500 m/s. The solid contour lines correspond to the exact summation surface, while the dashed contour lines correspond to the approximate summation surface. biondo1-planecheops [ER]

same contour lines in plane view. The solid lines correspond to the exact summation surface, while the dashed lines correspond to the approximate summation surface. Figure 1 graphically demonstrates that even in constant velocity, offset plane wave migration introduces an error for reflectors that are not exactly dipping in either the in-line direction or the cross-line direction.

The analysis of the offset plane wave migration impulse response, or spreading surface, provides an alternative perspective to the analysis of the migration errors. The spreading surface of full 3-D prestack migration is the ellipsoid:

$$\frac{4\left(x_\xi - x_m\right)^2}{t_D^2 V^2} + \frac{4\left(y_\xi - y_m\right)^2}{t_D^2 V^2 - 4h^2} + \frac{4z_\xi^2}{t_D^2 V^2 - 4h^2} = 1. \tag{16}$$

It can be split as the cascade of the in-line prestack migration ellipse:

$$\frac{4\left(x_\xi - x_m\right)^2}{t_D^2 V^2} + \frac{4z_x^2}{t_D^2 V^2 - 4h^2} = 1, \tag{17}$$

and the cross-line zero-offset semicircle:

$$\frac{\left(y_\xi - y_m\right)^2}{z_x^2} + \frac{z_\xi^2}{z_x^2} = 1. \tag{18}$$

The impulse response of offset plane wave migration, as defined by the dispersion relation in equation (8), is defined by the cascade of the following two impulse responses

$$\frac{4\left(y_\xi - y_m\right)^2}{t_D^2 V^2} + \frac{z_{\bar{y}}2}{t_D^2 V^2} = 1, \tag{19}$$

$$\frac{4\left(x_\xi - x_m\right)^2}{z_{\bar{y}}^2} + \frac{4z_\xi^2}{z_{\bar{y}}^2 - 4h^2} = 1. \tag{20}$$

Figure 2 compares the exact impulse response of 3-D prestack migration and the offset plane wave approximation. The grey surface shown in the left panel of Figure 2 is the exact spreading surface for an impulse recorded at 2.5 s, at an offset of 4,000 m, and assuming a constant velocity of 2,500 m/s. The inner set of contour lines corresponds to the exact summation surface, while the outer one corresponds to the surface defined by cascading the paths defined in equation (19) and equation (20). The right panel of Figure 2 shows the same contour lines in plane view. The solid lines correspond to the exact spreading surface, while the dashed lines correspond to the approximate spreading surface. It is apparent that the approximation is worse for shallow reflectors dipping at 45 degrees with respect to the acquisition axes. This qualitative analysis is confirmed by the numerical results shown in the next section.

At zero offset the order of the in-line and cross-line migrations is obviously irrelevant; it is intuitive that the errors introduced by reversing the correct migration order increases with offset. To analyze the errors as a function of offset, Figure 3 compares the exact impulse response of 3-D prestack migration and the offset plane wave approximation at an offset of 8,000 m, and assuming the same constant velocity as in Figure 2 (2,500 m/s). The left panel of Figure 3 shows the exact spreading surface for an impulse recorded at 3.73 s. To make Figure 3 directly comparable with Figure 2, the impulse time was chosen to locate the bottom of the ellipsoid at exactly the same depth as in Figure 2, and the contour lines were drawn at the same depths as in Figure 2. It is apparent that at constant reflector depth the errors increase as the offset increases.

MIGRATION RESULTS OF THE SEG-EAGE SALT DATA SET

In the previous two sections I have analyzed the theoretical differences between common-azimuth migration and offset plane wave migration. In this section, I compare the migration results.

The theoretical analysis identified two approximations that are made in offset plane wave migration: first, the setting of the cross-line offset ray parameter to zero, and second, downward continuing the offset plane waves separately, when in lateral varying media they should be allowed to mix. To enable the independent analysis of the effects of both approximations, I run three migration programs:

(A) Common-azimuth migration

(B) Hybrid offset plane wave migration (with plane-wave mixing)

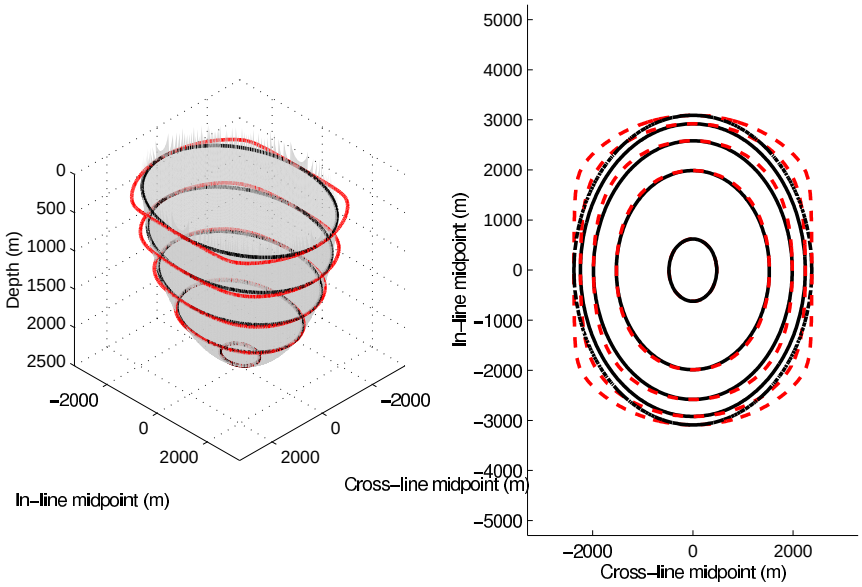

Figure 2: The grey surface shown in the left panel is the exact spreading surface for an impulse at at 2.5 s, an offset of 4,000 m, and assuming a constant velocity of 2,500 m/s. The solid contour lines correspond to the exact spreading surface, while the dashed contour lines correspond to the approximate spreading surface. biondo1-planeellips [ER]

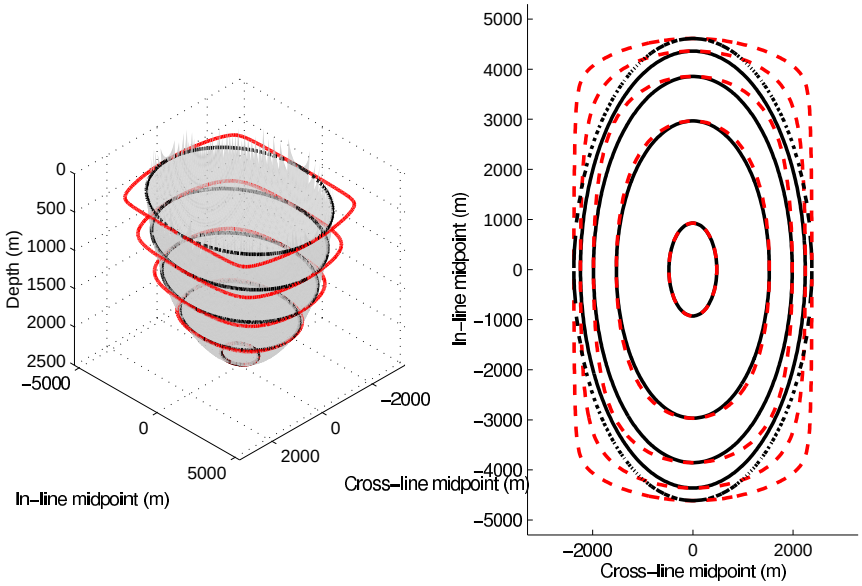

Figure 3: The grey surface shown in the left panel is the exact spreading surface for an impulse at at 3.73 s, an offset of 8,000 m, and assuming a constant velocity of 2,500 m/s. The solid contour lines correspond to the exact spreading surface, while the dashed contour lines correspond to the approximate spreading surface. biondo1-planeellips8km [ER]

(C) Offset plane wave migration (without plane-wave mixing).

All three programs implement the downward-continuation operators in the frequency-wavenumber domain and adapt to lateral velocity variations by an extended split-step method (Stoffa et al., 1990). When required, the offset-plane wave decomposition was performed inside the migration by Fourier transforms, relying on the well-known relations between ray parameters and wavenumbers ($p_{x_h} = k_{x_h}/\omega$ and $p_{y_h} = k_{y_h}/\omega$). Both the offset plane wave migration (C) and the hybrid offset plane wave migration (B) apply the dispersion relation in equation (8). The only difference between the two is that in (C) the offset-wavenumber axis is not transformed into the space domain when applying the split-step correction; that is, each offset-wavenumber (plane-wave) component is downward continued independently for all depths. On the other hand, the only difference between migration (A) and migration (B) is that in migration (B) the cross-line offset wavenumber was set to zero, while in migration (A) it was evaluated using equation (3).

The input data set was the same for all three programs, and the same as I used for my previous comparison of common-azimuth migration and Kirchhoff migration (Biondi, 1999a). The Salt Model C3-NA data set (SEG-EAGE, 1997; Clapp et al., 1999) was transformed to effective common-azimuth data by applying Azimuth Moveout (Biondi et al., 1998). The regularized common-azimuth data set was binned with a 20 meter CMP spacing in both the in-line and cross-line directions, and with 100 meter sampling along the in-line offset direction. The data were muted with a "deep" mute because the early arrivals are contaminated by all sorts of modeling noise. This mute affected the imaging of the shallow events. A more careful mute could accomplish both noise removal and shallow event preservation.

With respect to the previous tests, I increased the number of reference velocities from four to six. I wanted to verify the hypothesis that the poor imaging of a fault by common-azimuth migration was caused by having used too few reference velocities (Figure 5 in the previous report). Indeed, the fault is much better imaged when six reference velocities are used (Figure 10 in this report).

Comparison of common-azimuth migration with hybrid offset plane wave migration

The comparison of the constant-velocity migration operators presented in the previous sections indicates that the errors introduced by setting the cross-line offset ray parameter to zero are the largest for relatively shallow reflectors. Confirming the theoretical analysis, the differences between the images produced by common-azimuth migration (A) and the hybrid offset plane wave migration (B) are the largest in the shallow part of the image. Reflections from faults above the salt body and the salt flanks are affected when their dips are oriented at about 45 degrees with respect to the acquisition axes. In the sub-salt area there are no noticeable differences between the results produced by migrations (A) and (B). However, because this synthetic data set has a short maximum offset (2.4 km), these results are not necessarily indicative of migration performances for sub-salt imaging of real data sets, that are usually collected with much longer maximum offsets (4-6 km).

The next four figures compare the upper portion (down to a maximum depth of 1,500 m) of two in-line sections and two cross-line sections obtained by migrations (A) and (B). Figure 4 compares the in-line sections obtained by common-azimuth migration (A) and the hybrid offset plane wave migration (B). Migration (B) fails to image properly segments of the two large faults above the salt body. The image degradation is larger for the lower parts of the faults, contrary to the expectations induced by the theoretical analysis presented in the previous section. The relatively small degradation of the shallower parts of the faults can be explained by the muting applied to the early arrivals in the data. This muting reduced the effective maximum offset of the early reflections and thus decreased the errors introduced by offset plane wave migration. Further investigations of this aspect of the results are warranted.

Figure 5 compares the in-line sections obtained by common-azimuth migration (A) and the hybrid offset plane wave migration (B). The left flank of the salt body is better imaged by migration (A) than by migration (B). Migration (B) fails also to focus properly the ridge on the top of the salt visible in panel a) at in-line location of about 7,000 m.

Figure 6 compares the cross-line sections obtained by common-azimuth migration (A) and the hybrid offset plane wave migration (B). Both the right and left flank of the salt are better imaged by migration (A) than by migration (B). Migration (A) produces also a better image of the fault located at cross-line location of about 6,000 m

Figure 7 compares the cross-line sections obtained by common-azimuth migration (A) and the hybrid offset plane wave migration (B). Again, migration (B) fails to image the lower segment of the fault located at cross-line location of about 6,000 m, and the ridge on the top of the salt located at cross-line location of about 8,000 m. Notice that this is the same ridge visible in the in-line sections shown in Figure 5.

Comparison of common-azimuth migration with offset plane wave migration

The velocity above the salt body does not vary rapidly in the lateral directions. Therefore the images obtained by the hybrid offset plane wave migration (B) and the "real" offset plane wave migration (C) are very similar. On the contrary, below the salt body, the approximation introduced by downward-continuing the offset plane wave separately causes significant problems in the imaging of the sub-salt reflectors. The next four figures compare the deeper portion (starting from a minimum depth of 1,500 m) of two in-line sections and two cross-line sections obtained by migrations (A) and (C). The sub-salt images are considerably noisier than the above-salt images. To facilitate the analysis, I show also the corresponding sections of the velocity model.

Figure 8 compares the in-line sections obtained by common-azimuth migration (A) and the offset plane wave migration (C); Figure 9 shows the corresponding section of the velocity model. The bottom of the salt body, and in particular the dipping segment at the left edge of the salt, is better imaged by migration (A) than by migration (C). In the shadow of the salt body, the image of the basement is also more continuous in panel a) than in panel b).

Figure 10 compares the in-line sections obtained by common-azimuth migration (A) and

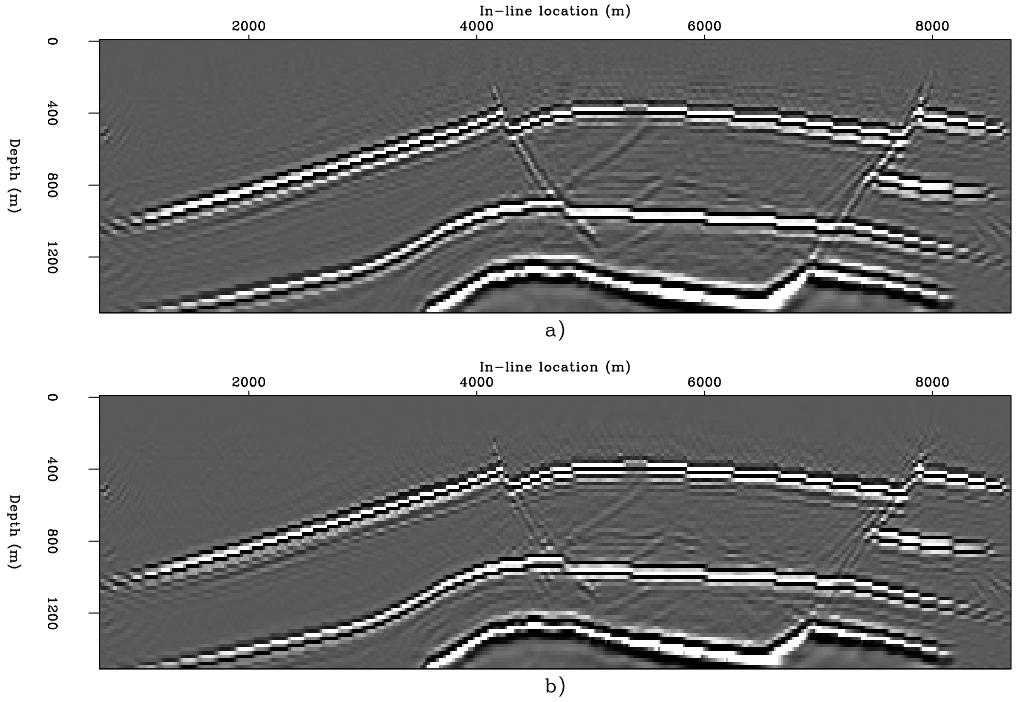

Figure 4: In-line sections (cross-line location 5,990 m) from the images obtained with a) common-azimuth migration (A), b) the hybrid offset plane wave migration (B). biondo1-Both-salt-over-x5990 [CR]

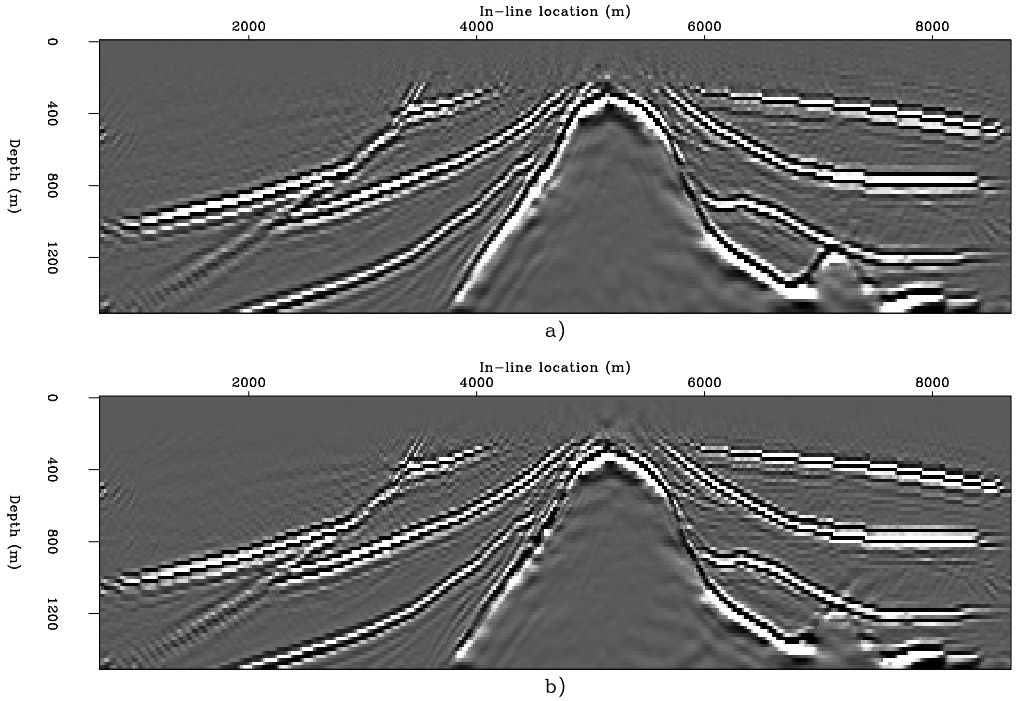

Figure 5: In-line sections (cross-line location 8,070 m) from the images obtained with a) common-azimuth migration (A), b) the hybrid offset plane wave migration (B). biondo1-Both-salt-over-x8070 [CR]

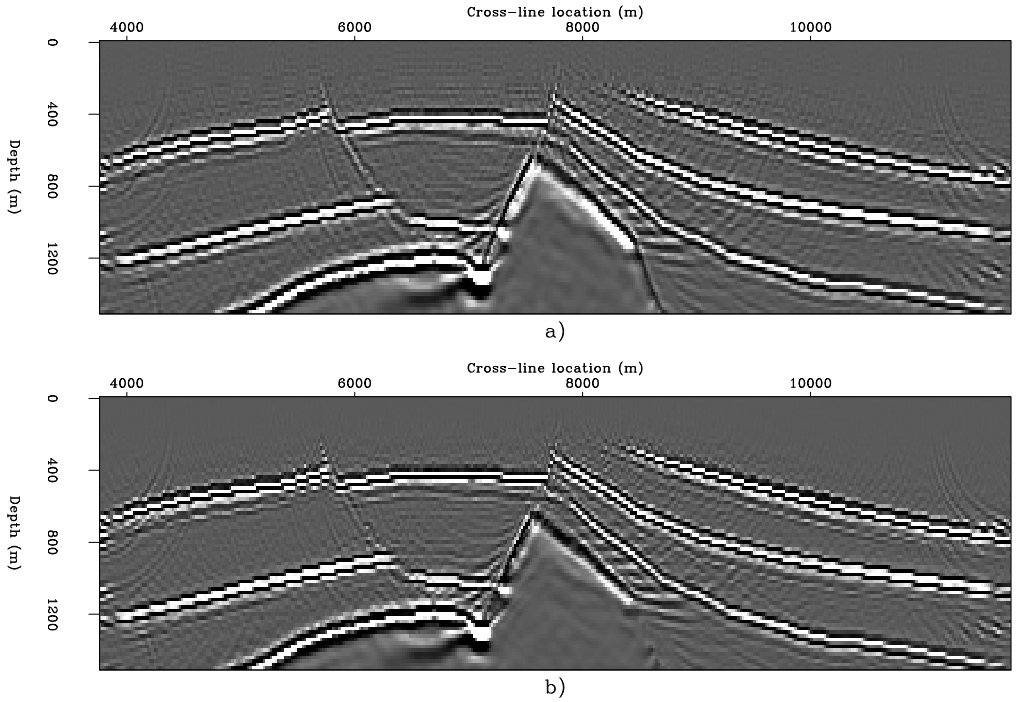

Figure 6: Cross-line sections (in-line location 4,420 m) from the images obtained with a) common-azimuth migration (A), b) the hybrid offset plane wave migration (B). biondo1-Both-salt-over-y4420 [CR]

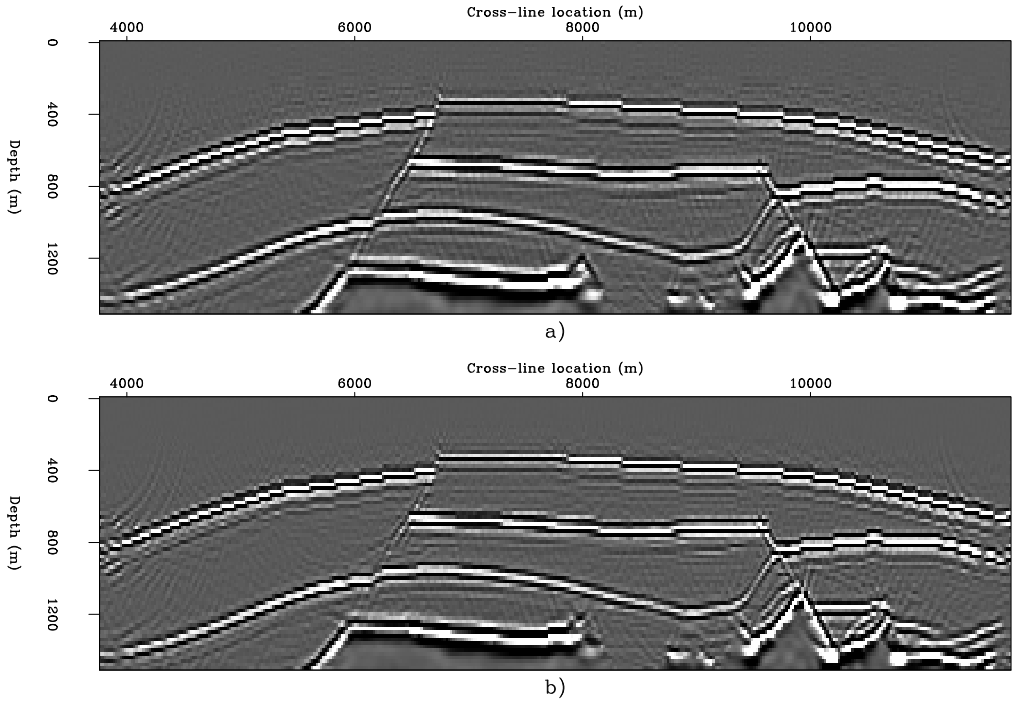

Figure 7: Cross-line sections (in-line location 6,960 m) from the images obtained with a) common-azimuth migration (A), b) the hybrid offset plane wave migration (B). biondo1-Both-salt-over-y6960 [CR]

the offset plane wave migration (C); Figure 11 shows the corresponding section of the velocity model. Both sand lenses visible in the right part of the sections are better imaged by migration (A) than by migration (C); in particular, the deeper lens just above the basement reflector is more clearly defined in panel a) than in panel b). The image of the basement is also more continuous in panel a) than in panel b). Possibly the most interesting difference is in the imaging of the anticlinal structure broken by converging normal faults visible in between the two sand lenses. Migration (A) produces an image, though fairly faint, of this structure even in the shadow of the salt body. In contrast, the structure disappears from the image produced by migration (C) as soon as it gets in the shadow of the salt body.

Figure 12 compares the cross-line sections obtained by common-azimuth migration (A) and the offset plane wave migration (C); Figure 13 shows the corresponding section of the velocity model. The dipping segment of the bottom of the salt that belongs to the fault plane cutting through the salt body (cross-line location 8,000 m) is better imaged by migration (A) than by migration (C). The basement reflector is also more continuous in panel a) than in panel b).

Figure 14 compares the cross-line sections obtained by common-azimuth migration (A) and the offset plane wave migration (C); Figure 15 shows the corresponding section of the velocity model. As for the in-line sections shown in Figure 10, both sand lenses visible in the right part of the sections are better imaged by migration (A) than by migration (C). Though discontinuous in places, the basement reflector is also better imaged by migration (A) than by migration (C). The bottom of the salt reflector right below the deep canyons in the salt body (in-line location 8,000-9,200 m) is fairly coherent in panel a), while it is discontinuous in panel b).

CONCLUSIONS

Both offset plane wave migration and common-azimuth migration are computationally efficient wave-equation methods to image marine 3-D prestack data. Offset plane wave migration introduces approximations that are avoided by common azimuth migration. The theoretical analysis and the imaging comparison presented in this paper produce a convincing and consistent analysis of the migration errors caused by these approximations.

The approximation that is most detrimental to sub-salt imaging is caused by downward-continuing the offset plane waves separately. In lateral varying media, wave-propagation theory predicts that plane-wave components should mix at every depth step. It is difficult to study analytically the effects of this approximation. But the imaging results show a consistent deterioration of sub-salt image quality when plane-wave components were not allowed to mix during the downward-continuation process.

The effects of setting the cross-line offset ray parameter to zero can be studied analytically, at least under the simplifying assumption of constant migration velocity. The fundamental insight for the theoretical analysis is provided by the decomposition of the dispersion relations used for common-azimuth migration and offset plane wave migration in the cascades of two

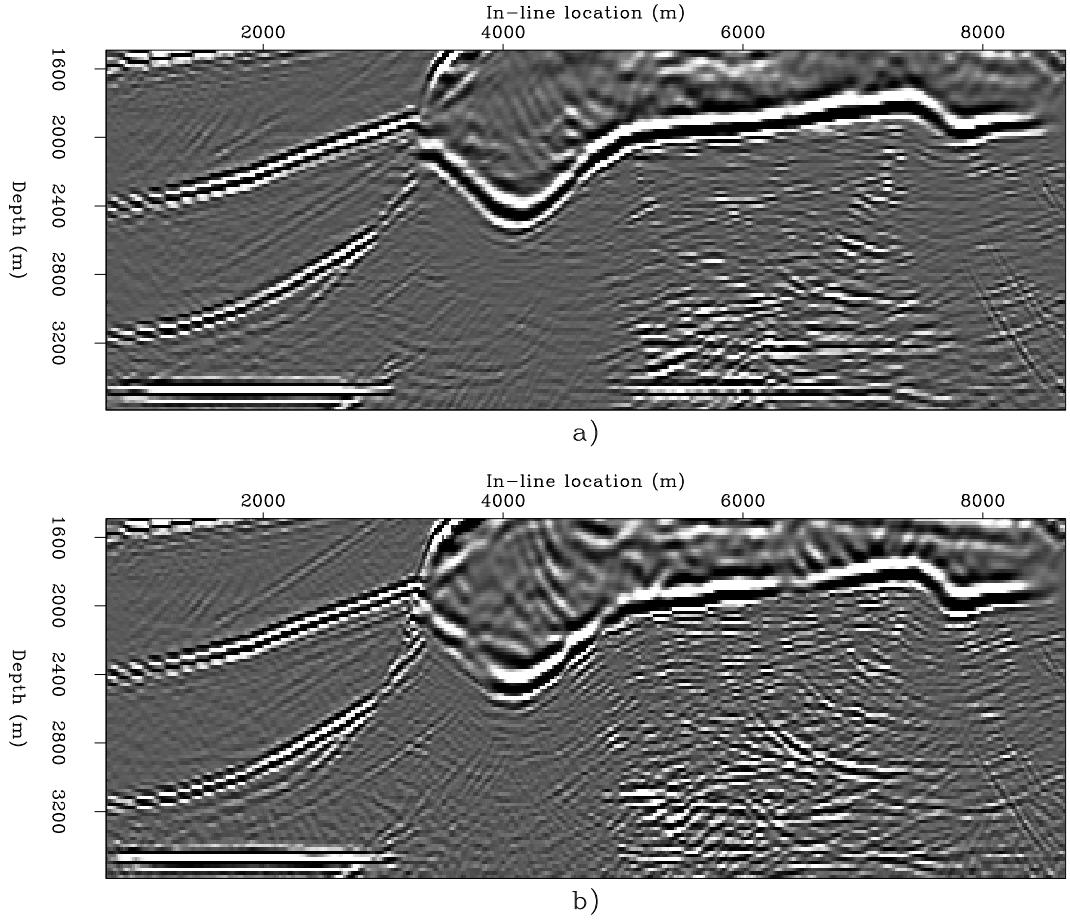

Figure 8: In-line sections (cross-line location 6,300 m) from the images obtained with a) common-azimuth migration (A), b) offset plane wave migration (C). biondo1-Both-salt-under-x6300 [CR]

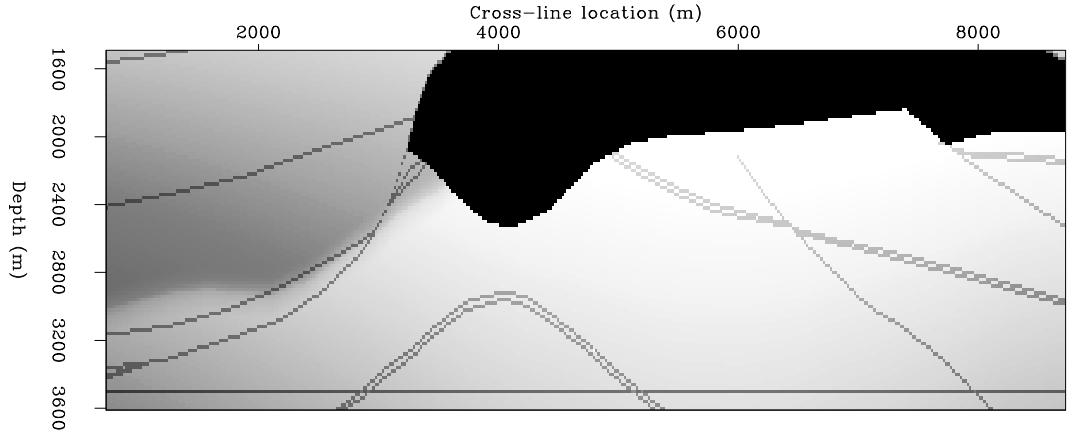

Figure 9: In-line section of the velocity model at cross-line location 6,300 m. biondo1-Vel-salt-under-x6300 [CR]

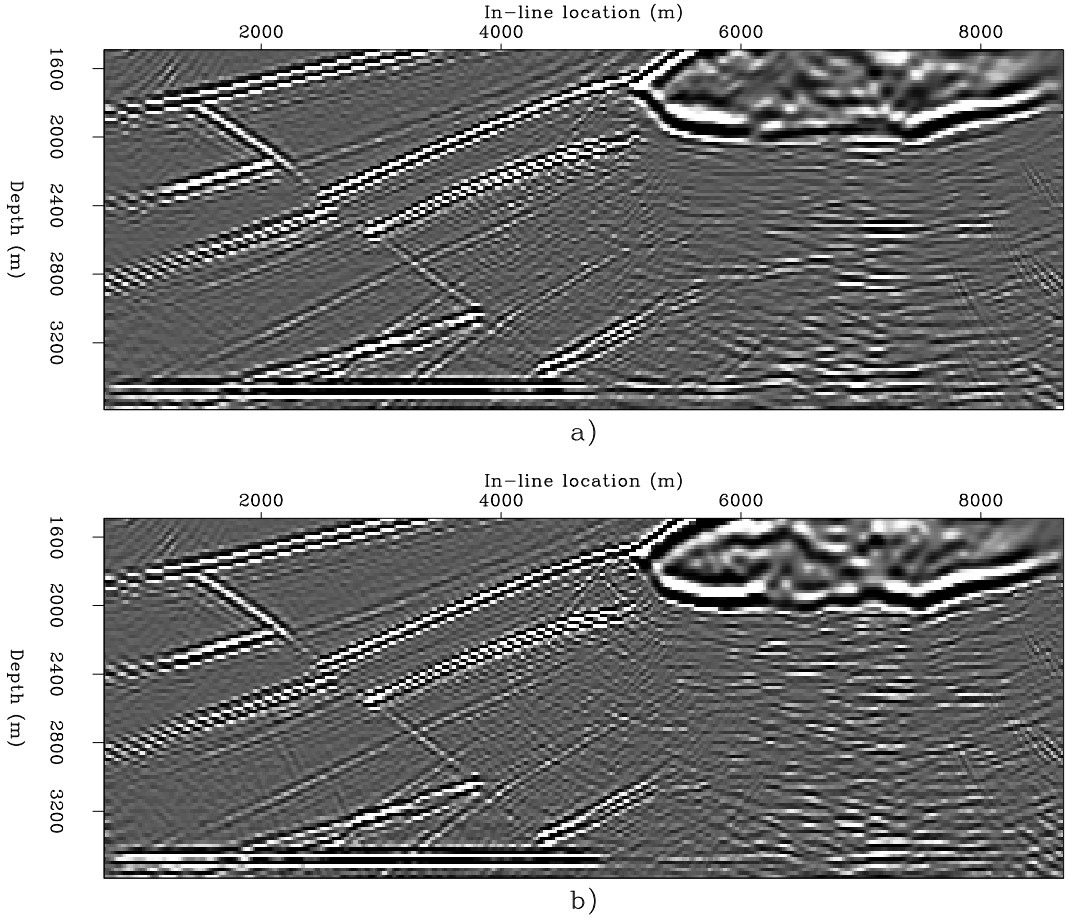

Figure 10: In-line sections (cross-line location 9,980 m) from the images obtained with a) common-azimuth migration (A), b) offset plane wave migration (C). biondo1-Both-salt-under-x9980 [CR]

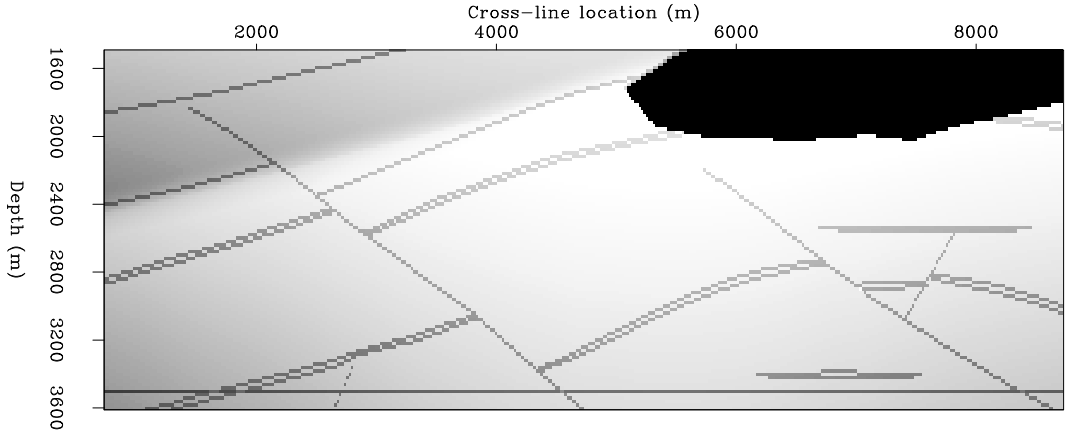

Figure 11: In-line section of the velocity model at cross-line location 9,980 m. biondo1-Vel-salt-under-x9980 [CR]

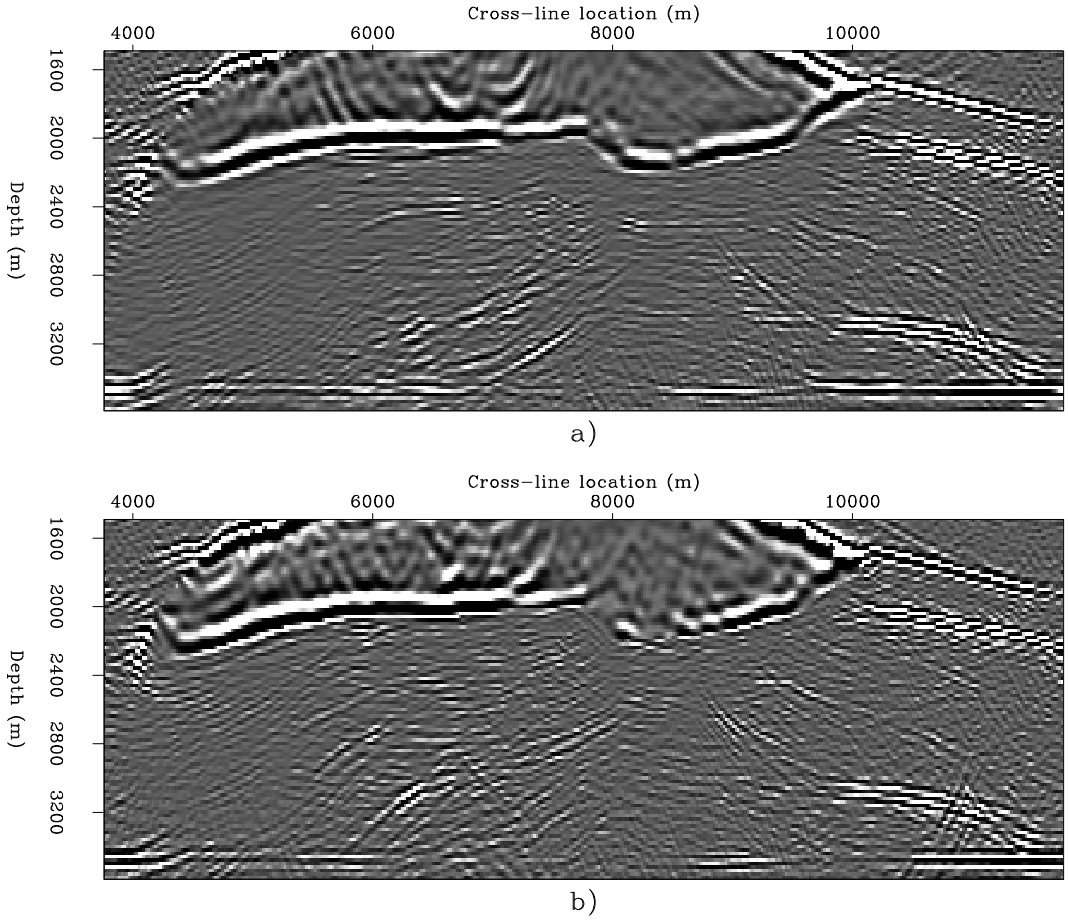

Figure 12: Cross-line sections (in-line location 5,180 m) from the images obtained with a) common-azimuth migration (A), b) offset plane wave migration (C). biondo1-Both-salt-under-y5180 [CR]

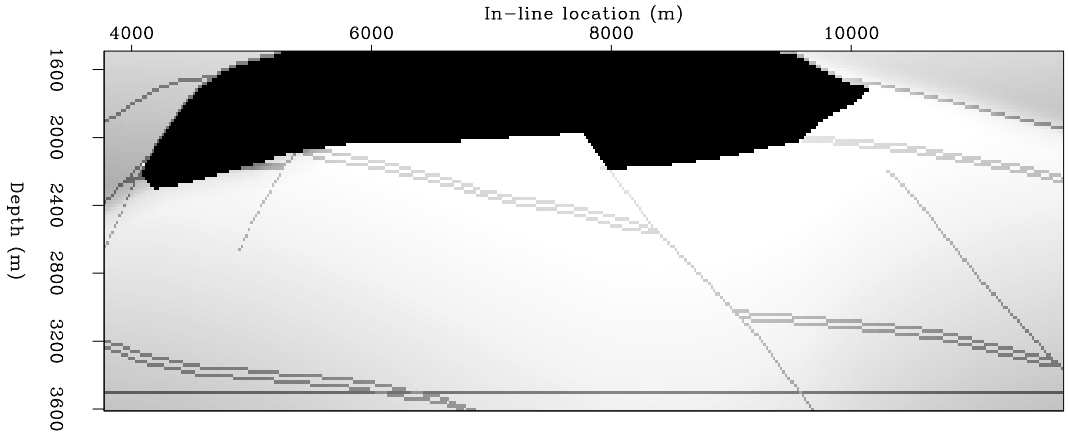

Figure 13: Cross-line section of the velocity model at in-line location 5,180 m. biondo1-Vel-salt-under-y5180 [CR]

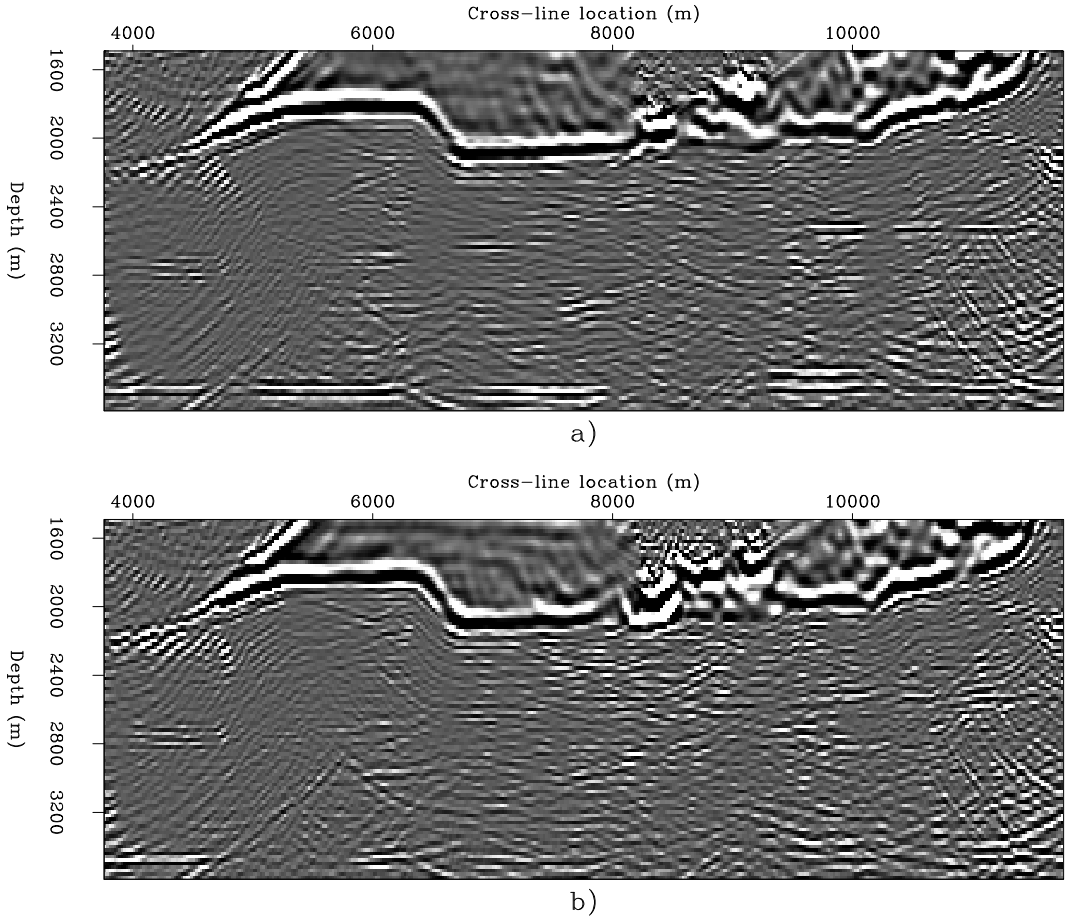

Figure 14: Cross-line sections (in-line location 7,300 m) from the images obtained with a) common-azimuth migration (A), b) offset plane wave migration (C). biondo1-Both-salt-under-y7300 [CR]

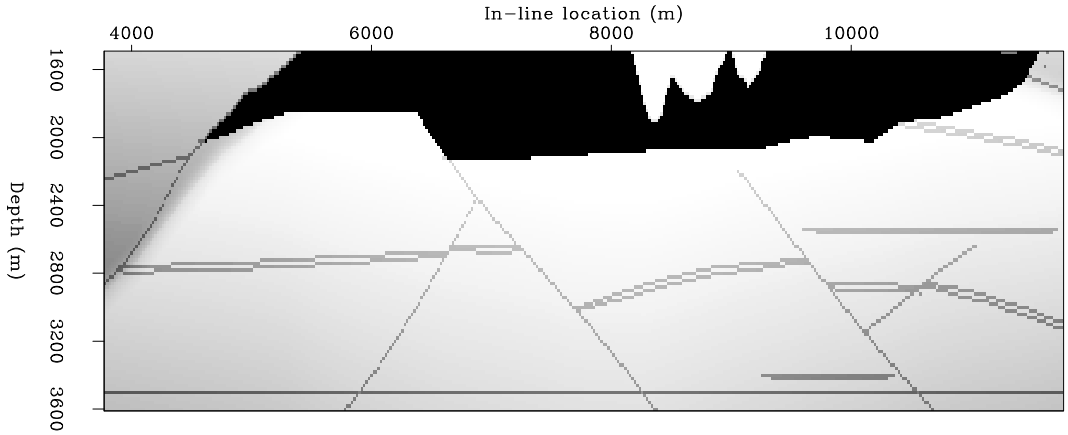

Figure 15: Cross-line section of the velocity model at in-line location 7,300 m. biondo1-Vel-salt-under-y7300 [CR]

dispersion relations. This decomposition yields to a straightforward evaluation of the equivalent constant-velocity migration operators.

The imaging results confirm the predictions of the theoretical analysis that the shallow reflectors dipping at 45 degrees with respect to the acquisition axes are the most affected by this approximation. On the contrary, this approximation does not seem to have affected the imaging results of the deeper reflectors. However, my theoretical analysis predicts that the errors introduced by this approximation increase with offsets, and the synthetic data set used for this study has a shorter maximum offset (2.4 km) than data sets routinely recorded for sub-salt imaging (4-6 km). Therefore, the results presented in this paper are not conclusive to determine whether the imaging of deeper reflectors would be satisfactory with real data.

Offset plane-wave migration has some potential computational advantages with respect to common-azimuth migration. Therefore, the results presented in this paper indicate it could be a cost-effective migration method to produce full-volume images of deep targets below relatively mild velocity functions. Though more expensive, common-azimuth migration should produce better images below complex overburden (e.g. below salt bodies) and when shallow dipping reflectors are important to the overall interpretation.

ACKNOWLEDGEMENTS

This research was partially funded by the ACTI project # 4731U0015-3Q.

REFERENCES

Biondi, B., and Palacharla, G., 1996, 3-D prestack migration of common-azimuth data: Geophysics, **61**, no. 6, 1822–1832.

Biondi, B., Fomel, S., and Chemingui, N., 1998, Azimuth moveout for 3-D prestack imaging: Geophysics, **63**, no. 2, 574–588.

Biondi, B., 1999a, Subsalt imaging by common-azimuth migration: SEP–**100**, 113–124.

Biondi, B. L., 1999b, 3-D Seismic Imaging: `http://sepwww.stanford.edu/sep/biondo/Lectures/index.html`.

Clapp, R. G., Brown, M., Vaillant, L., Mora, C., Prucha, M., and Zhao, Y., 1999, SEP Data Library: `http://sepwww.stanford.edu/pub/docs/sepdatalib/toc_html/`.

Mosher, C. C., Foster, D. J., and Hassanzadeh, S., 1997, Common angle imaging with offset plane waves: 67th Annual Internat. Mtg., Soc. Expl. Geophys., Expanded Abstracts, 1379–1382.

Ottolini, R., and Claerbout, J. F., 1984, The migration of common-midpoint slant stacks: Geophysics, **49**, no. 3, 237–249.

Rosa, A., Cunha, C., Pedrosa, I., Panetta, J., Sinedino, S., and Braga, V., 1999, Two-pass 3-D prestack time migration: 6th Internat. Congr. Braz. Geophys. Soc., SBGf, RIO 99, CD–ROM.

SEG-EAGE, 1997, Salt Model Narrow-Azimuth Classic dataset (C3-NA): `http://archive.llnl.gov/SSD/classic/classicSalt.html#salt-c`.

Stoffa, P. L., Fokkema, J. T., de Luna Freire, R. M., and Kessinger, W. P., 1990, Split-step Fourier migration: Geophysics, **55**, no. 4, 410–421.

Stolt, R. H., 1978, Migration by Fourier transform: Geophysics, **43**, no. 1, 23–48.

Vaillant, L., and Sava, P., 1999, Common-azimuth migration of a north sea dataset: SEP–**102**, 1–14.